Hydrogeology Journal (2022) 30:767–782
https://doi.org/10.1007/s10040-022-02470-z

REPORT

Groundwater response to climate variability in Mediterranean type climate zones with comparisons of California (USA) and Portugal

Katherine A. Malmgren[1] · Maria C. Neves[1,2] · Jason J. Gurdak[3] · Luis Costa[1,4] · José P. Monteiro[1,4]

Received: 26 March 2021 / Accepted: 21 February 2022 / Published online: 31 March 2022

Abstract

Aquifers are a fundamental source of freshwater, yet they are particularly vulnerable in coastal regions with Mediterranean type climate, due to both climatic and anthropogenic pressures. This comparative study examines the interrelationships between ocean-atmosphere teleconnections, groundwater levels and precipitation in coastal aquifers of California (USA) and Portugal. Piezometric and climate indices (1989–2019) are analyzed using singular spectral analysis and wavelet transform methods. Singular spectral analysis identifies signals consistent with the six dominant climate patterns: the Pacific Decadal Oscillation (PDO), the El Niño-Southern Oscillation (ENSO), and the Pacific/North American Oscillation (PNA) in California, and the North Atlantic Oscillation (NAO), the Eastern Atlantic Oscillation (EA) and the Scandinavian Pattern (SCAND) in Portugal. Lower-frequency oscillations have a greater influence on hydrologic patterns, with PDO (52.75%) and NAO (46.25%) on average accounting for the largest amount of groundwater level variability. Wavelet coherences show nonstationary covariability between climate patterns and groundwater levels in distinct period bands: 4–8 years for PDO, 2–4 years for ENSO, 1–2 years for PNA, 5–8 years for NAO, 2–4 years for EA and 2–8 years for SCAND. Wavelet coherence patterns also show that coupled climate patterns (NAO+ EA– and paired PDO and ENSO phases) are associated with major drought periods in both the Mediterranean climate zones.

Keywords Coastal aquifers · Climate change · Groundwater level · Ocean-atmosphere teleconnections · USA · Portugal

Introduction

Groundwater is a subsurface freshwater resource that acts as an essential buffer to meet domestic and irrigation demands particularly during periods of drought (Gurdak 2017; Russo and Lall 2017). Large-scale droughts, however, can severely compromise groundwater supply. Outstanding examples of multiyear drought with pronounced land-use change in the Great Plains of the United States spurred the Dust Bowl in the 1930s with similar conditions propagating today (Schubert et al. 2004; Romm 2011). Sahelian droughts of the 1970s and 1980s devastated Africa, as climate variability patterns and low recharge rates, ranging from 0.1 to 5% of annual precipitation, restricted groundwater availability (Giannini et al. 2003; Scanlon et al. 2006; Masih et al. 2014). Groundwater storage in Australia's Murray–Darling Basin declined by ~100 ± 35 km^3 from 2000 to 2007 during the Millennium Drought (Taylor et al. 2013). Today, over 2 billion people rely on groundwater as their primary source of freshwater (Kundzewicz and Döll 2009) and 1.7 billion people live in water-stressed areas (Gleeson et al. 2012). Aquifers in semi-arid regions, including the Mediterranean (Giorgi 2006; Stigter et al. 2014) and the southwestern US (Barco et al. 2010; Manna et al. 2019), are particularly vulnerable to climate change (Navarra and Tubiana 2013; Cui et al. 2020) and natural climate variability (Taylor et al. 2013; Cui et al. 2017). Moreover, two thirds of the world's population inhabit coastal areas (United Nations 2016) making coastal aquifers in

✉ Katherine A. Malmgren
kamalmgren@ualg.pt

[1] Faculdade de Ciências e Tecnologia, Universidade do Algarve Campus de Gambelas, 8005-139 Faro, Portugal

[2] Instituto Dom Luiz (IDL), Universidade de Lisboa, 1749-016 Lisbon, Portugal

[3] Dept. of Earth and Climate Sciences, San Francisco State University, San Francisco, CA, USA

[4] Centro de Ciências e Tecnologia da Água, Universidade do Algarve, Campus de Gambelas, 8005 139 Faro, Portugal

semiarid areas more susceptible to excessive anthropogenic activities such as overabstraction and population inflation from tourism.

Natural climate variability on time scales varying from several years to several decades is driven by large-scale atmospheric and oceanic circulation patterns, also known as teleconnections. Ocean-atmosphere oscillation patterns such as for example, the El Niño Southern Oscillation (ENSO), Pacific Decadal Oscillation (PDO), North Atlantic Oscillation (NAO) and East Atlantic pattern (EA), are associated with interannual to multidecadal fluctuations of precipitation, temperature, streamflow, and snowmelt (Beebee and Manga 2004; Brabets and Walvoord 2009; Ropelewski and Halpert 1986; Trigo et al. 2008; Vicente-Serrano et al. 2011). As teleconnections alter hydrological budgets, their impact on aquifers has been recognized throughout the world (Holman et al. 2011; del V Venencio and García 2011; Tremblay et al. 2011; De Vita et al. 2012; Perez-Valdivia et al. 2012; Asoka et al. 2017; Joshi et al. 2020). In Portugal, dominant climate patterns drive most (80%) of groundwater variability (Neves et al. 2019b) and over 80% in the California Coastal Basins aquifers (USA), that are not directly influenced by anthropogenic stresses such as pumping or managed aquifer recharge (Kuss and Gurdak 2014; Velasco et al. 2017).

Couplings or superpositions of large-scale climate patterns, as well as temporal shifts in their synchronization, may lead to hydrological extremes (Cleverly et al. 2016; Neves et al. 2019b) and offer an opportunity for potential recurrent drought prediction (Rust et al. 2019; Fan et al. 2020). However, while links between climate variability and groundwater levels have been identified in several parts of the world, little is known about the implications of complex couplings among modes, and their connection to droughts, which is pertinent to understanding future recharge and groundwater availability, especially in already water-stressed areas such as coastal Mediterranean regions. Recent studies have presented results on teleconnection interactions across various domains, including groundwater level fluctuations (Corona et al. 2018; Neves et al. 2019a, b; Velasco et al. 2017) and drought extent (Jolly et al. 2015; Liu et al. 2010; Norman and Taylor 2003)—for example, the combined effects of the positive phase of NAO (NAO+) and the negative phase of EA (EA–) has extended drought severity and period in Portugal (Neves et al. 2019b; Trigo et al. 2013). Synchronized patterns can determine heat transfer, surface water and groundwater flows across Europe (Holman et al. 2011; Kalimeris et al. 2017; Steirou et al. 2017). A positive PDO phase can intensify El Niño, driving a more robust pattern of wetter winters in the southern US. (Gershunov and Barnett 1998). Coupling events can also modify the placement of climate variability patterns spatially, constraining effects at a smaller regional.

This work is the first to provide a comparative statistical and analytical analysis of the impact of climate patterns, and their couplings, on coastal Mediterranean aquifers on two different continents. An investigation of coastal groundwater response to climate variability in two West Coast aquifer systems—California (USA) and Portugal—is selected due to their similarities within a prevailing Mediterranean climate zone and the overall vulnerability of groundwater systems in these climates globally. The main research questions here are: How do groundwater level fluctuations and interannual climate variability compare in Portugal and California? Is there a common response to climate pattern couplings? What is the connection between mode couplings and drought? Although the specific geographic focus is the Mediterranean climate zone, the research on the impact of climate patterns on coastal aquifers, considering phase couplings and extreme weather events, is a novel line of research that is relevant to other semiarid regions of the world also increasingly threatened by droughts.

Materials and methods

Hydrogeologic site descriptions

This study evaluates the California Coastal Basins aquifers (CA; Fig. 1a) and several coastal aquifer systems of Portugal (PT; Fig. 1b). The US Geological Survey (USGS) classifies the California Coastal Basins system as a Principal Aquifer (PA) of the United States, which are generally unconfined and are formed from unconsolidated to semiconsolidated sand and gravel material, with characteristically moderate to high hydraulic conductivity (USGS 2015). The California Coastal Basins aquifers, located along the coast of California, are comprised of over 100 basin-fill aquifers predominantly composed of marine and alluvial sediments with some volcanic deposits, and examples of their geological cross sections can be found in (Planert and Williams 1995).

The four large morphostructural and corresponding hydrogeologic units of Portugal, as defined by the Instituto da Água (INAG), are the Hespéric Massif, the West and Southern Meso-Cenozoic Basins and Tejo-Sado Tertiary Basin. The northernmost selected aquifers develop on the West Meso-Cenozoic basin, which forms an elongated north-northeast–south-southwest (NNE–SSW) depression filled with sediments that can reach a thickness of up to 5 km. Main geological formations are comprised of Jurassic limestones, dolomites and marls and, to a less extent, sandstones, clays and marls from the Cretaceous. The southernmost aquifers are in the Meso-Cenozoic basin of the Algarve region, mostly characterized by Jurassic limestones, dolomites and marls, which outcrop further inland, sequenced by Miocene limestones and sandstones. A detailed description of the Portuguese aquifers with geological cross sections can be found in Almeida et al. (2000) and Neves et al. (2019a).

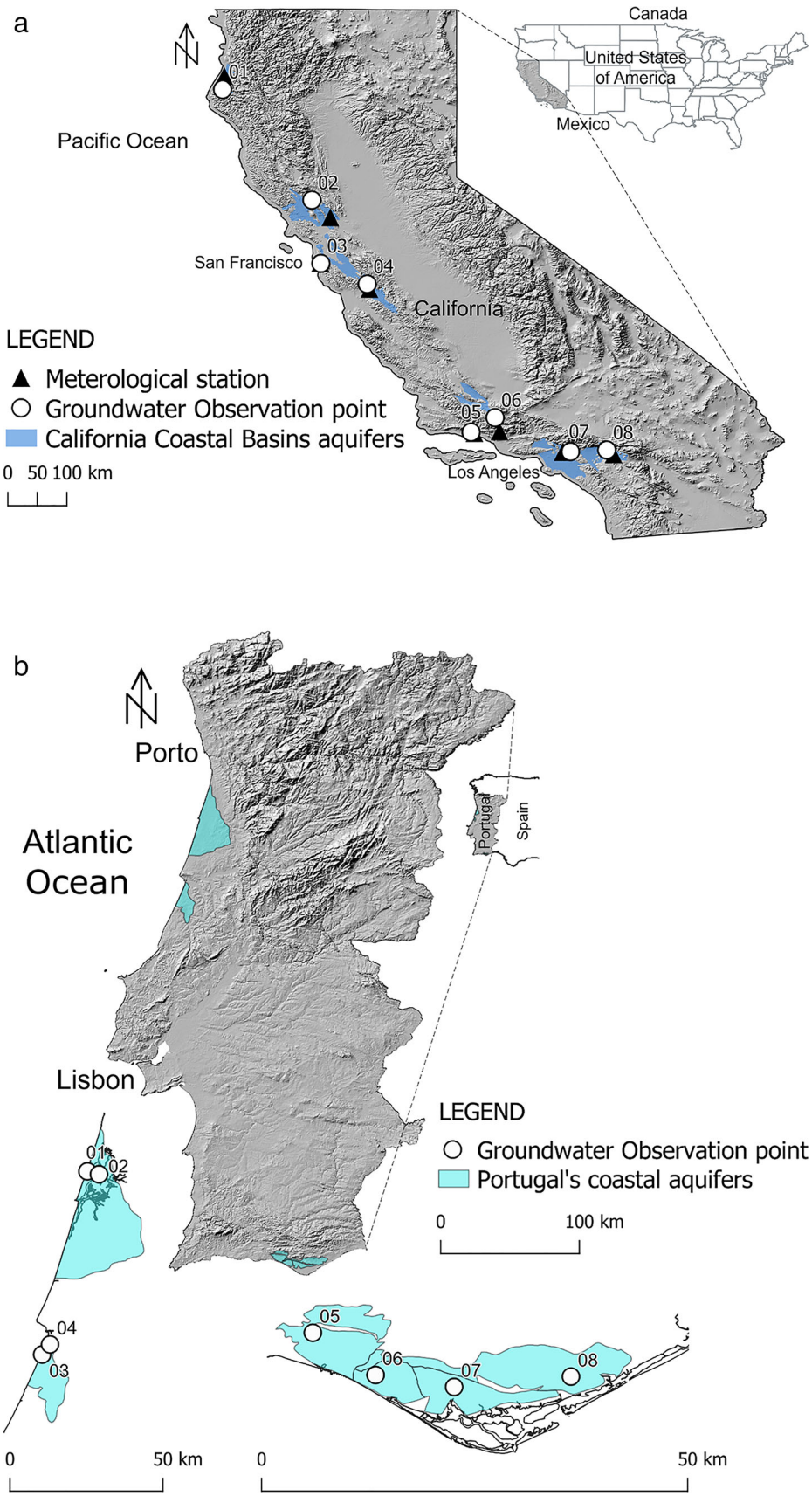

Fig. 1 **a** Map showing the location of precipitation and groundwater observation points in the California Coastal Basins aquifer system. **b** Map showing the location of groundwater observation points in Portugal's coastal aquifer system. Precipitation records and piezometers share the same coordinates and are therefore not displayed

Climatically, these coastal landmasses are classified as Mediterranean, with similar zonation from north to south, where about half of the annual precipitation arrives in a 3-month period from December through February (Miranda et al. 2002). Consequently, precipitation during wet winters determines the availability of water resources in the months that follow. Northwest Iberia and northern California are classified (Köppen-Geiger) as type Csb, temperate with dry and mild summers (Kottek et al. 2006). The Algarve region, in southern Portugal (SW Iberia), and central California are classified as type Csa, temperate with dry and hot summers, while southern California is arid to semiarid (Bwk). To make regional comparisons across the two prevailing climate zones, aquifer systems in each country were separated according to their location.

Climate variability

Climate patterns, or teleconnections, are seesaw-like fluctuations of major large-scale oceanic and atmospheric circulation modes. These patterns are characterized by indices which measure the strength of sea surface temperature and atmospheric pressure anomalies. Positive and negative phases of the indices, defined by values above or below given thresholds, are generally associated with either wet or dry conditions. Aquifers are inherently connected to modes of climate variability through precipitation and the hydrological cycle.

The leading climate patterns affecting the west coast of North America are the Pacific Decadal Oscillation (PDO), the El Niño-Southern Oscillation (ENSO), and the Pacific/North American Oscillation (PNA; Ghil 2002; McCabe et al. 2004; Kuss and Gurdak 2014; Velasco et al. 2017; Fig. 2a–c). ENSO is regarded as the most important interannual climate pattern globally (Palmer and Anderson 1994), is the largest signal driving North American climate (Gershunov et al. 1999) and has consequential environmental and socioeconomic impacts around the world (Bove et al. 1998; IPCC 2001; Mantua et al.,1997; Poveda et al. 2001). The PDO is associated with climate anomalies similar to ENSO producing comparable shifts in the jet stream (Mantua and Hare 2002). The PNA is associated with fluctuations in the strength and position of the East Asian jet stream, which is enhanced and shifted eastward towards the western US during the positive phase (Wallace and Gutzler 1981). The effect of ENSO, PDO and PNA on California's precipitation, as well as main periodicities associated with these climate pattern fluctuations, are summarized in Table 1. Positive (+) and negative (–) signs after the indices indicate the phase.

The dominant climate patterns affecting Portugal are the North Atlantic Oscillation (NAO), the East Atlantic Oscillation (EA), and the Scandinavian Pattern (SCAND; Fig. 2d–f). The NAO is a meridional dipole of pressure anomalies over southern Greenland (Icelandic Low) and the Azores (Azores High; Hurrell 1995) which exerts a primary control over winter precipitation in Portugal (Trigo et al. 2008). The EA is structurally similar to the NAO but is oriented to the southeast. In its positive phase, low pressure centers of EA are located over the North Atlantic, west of the British Isles, causing below-average precipitation over southern Europe (Barnston and Livezey 1987). The SCAND is center of action centered over the Scandinavian Peninsula and northeastern Atlantic and central Siberia (Bueha and Nakamurab 2007). The impacts of EA and SCAND patterns on precipitation regimes across Europe vary spatially and are inconsistent, whereas the NAO's influence is much more predictable (Trigo et al. 2008). The effect of NAO, EA and SCAND on Portugal's precipitation, as well as main periodicities associated with these climate pattern fluctuations, are also displayed in Table 1. However, when combined, the effects of NAO+ and EA– phases has extended drought severity and period in Portugal (Neves et al. 2019b; Trigo et al. 2013; Fig. 3) and synchronized NAO, EA, and SCAND can determine heat transfer, surface-water and groundwater flows in across Europe (Holman et al. 2011; Kalimeris et al. 2017; Steirou et al. 2017).

Hydrological data

The time series evaluated here include previously described climate indices (ENSO, PDO, PNA, NAO, EA and SCAND) and groundwater levels. Climate indices were obtained from NOAA's Climate Prediction Center for EA and SCAND (NOAA 2019), the National Center for Environmental Information (NCEI) for PDO, PNA and NAO (NOAA 2020a), and the Physical Sciences Laboratory (PSL) for ENSO (MEI.v2; NOAA 2020b).

Groundwater level time series for the selected sites, spanning the years of 1989–2019, were obtained from monitoring

Table 1 Dominant periods and synthesis of the hydrological implications of the positive phase (+) of six climate patterns pertinent to climate variability in California and Portugal: PDO, ENSO, PNA, NAO, EA, and SCAND. The negative phase has inverse effects. CA represents California, EU represents Europe

Climate pattern	Hydrological impact	Dominant periods
PDO+	↑ precipitation in S CA ↓ precipitation in N CA	15–30 years
ENSO+	↑ precipitation in S CA ↓ precipitation in N CA	2–7 years
PNA+	↓ precipitation in N CA	<1–4 years
NAO+	↑ precipitation in N EU ↓ precipitation in S EU	6–10 years
EA+	↑ precipitation in N EU ↓ precipitation in S EU	2–6 years
SCAND+	↓ precipitation in S EU	2–6 years

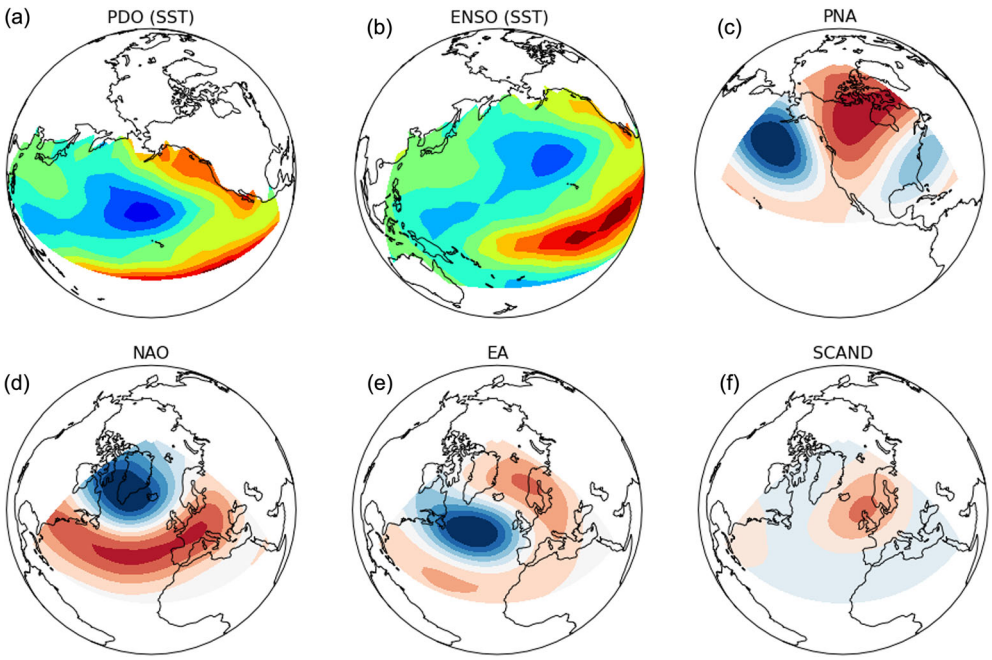

Fig. 2 Climate variability patterns and respective index temporal series. PDO and ENSO (**a**–**b**) are calculated using detrended monthly sea surface temperature (SST) anomalies. PNA, NAO, EA and SCAND (**c**–**f**) indices are spatial patterns of the first three empirical orthogonal functions of the 500 hPa geopotential height over the North American and European/Atlantic sector during wintertime. Both patterns and datasets were obtained from (NOAA 2019)

wells in the California Statewide Groundwater Elevation Monitoring (CASGEM) program's online public portal (CA DWR 2018) the USGS National Water Information System (NWIS; USGS 2015), and the Portuguese National System for Water Resources Information (SNIRH; APA 2020; Tables 2, 3, 4, and 5; Fig. 4). Monitoring wells within each aquifer

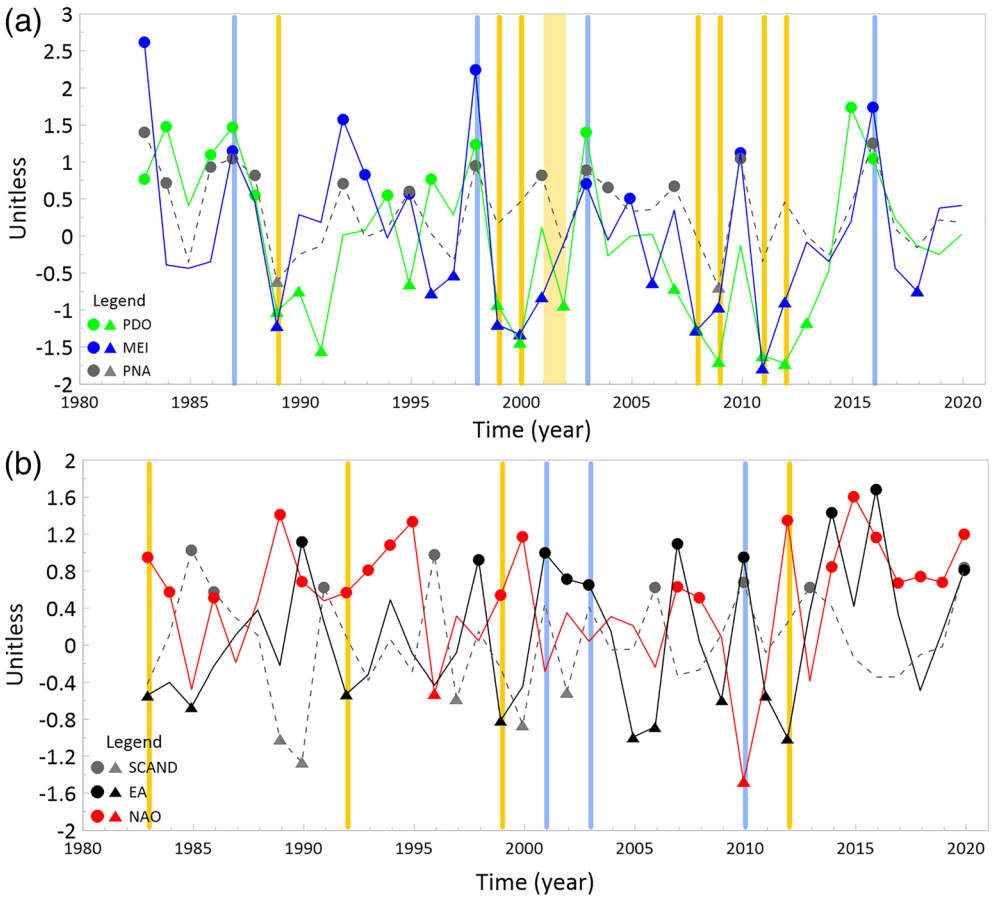

Fig. 3 Time series of the winter composites (December–March) of the climate indices in **a** California and **b** Portugal. Positive and negative phases of each index is defined by winter index values above 0.5 and below −0.5, respectively, and are marked by circle and triangle symbols. Color bars indicate major droughts and anomalous wet winters associated to phase couplings

system were selected based on criteria including the length and completeness of the record and contemporariness. A continuous record length of 30 years is assessed to capture interannual to interdecadal climate variability with at least a quarterly temporal resolution.

This study and others focusing on the impact of climate drivers (Velasco et al. 2017) try to use a selection of records not directly influenced by anthropogenic stresses such as pumping or managed aquifer recharge. Thanks to the California Sustainable Groundwater Management Act (CA SGMA), time series and record issues are documented through the Department of Water Resources. Site GW 02 in Napa is a residential well but a quality assurance description for the groundwater level measurement (questionable or no measurement), which may induce pumping, were not recorded during the study period. For the aquifers in Portugal, unfortunately, there are still no proper data on groundwater pumping, as most boreholes are privately owned and keep no abstraction records.

Methods of analysis

Analysis of the various time series is conducted using the USGS Hydrologic and Climatic Analysis Toolkit (HydroClimATe), which is a computer program that automates the use of several objective methods for assessing relations among hydrologic and climatic time series with spatial-temporal variability (Dickinson et al. 2014). This study uses HydroClimATe to preprocess the data and perform singular spectral analysis (SSA; Vautard et al. 1992; Ghil 2002).

Standard preprocessing steps such as treating outliers, interpolating missing values, detrending and normalization were conducted for all piezometers before the analysis. To have consistent monthly observations of piezometric level, the original time series were resampled to a monthly value and interpolated using quadratic interpolation. The detrended time series were standardized by the historic mean to form normalized departures (unitless) which allows for statistical comparisons among various data types. Analysis performed follows a systematized workflow, to first decompose the time series into reconstructed components using SSA, followed by the continuous wavelet transform (CWT) to expose dominant modes of variability with time evolving frequencies, and finally the wavelet coherence (WTC) to identify coupling events.

Singular spectral analysis is a form of principal component analysis used to examine long-term variations in noisy time series and is often applied to hydrologic time series (Enfield et al. 2001; Gurdak et al. 2007; Hanson et al. 2006; Kuss and Gurdak 2014; McCabe et al. 2004). Dominant frequencies representing the maximum possible amount of covariance are determined in a lagged covariance matrix by employing eigenanalysis (Broomhead and King 1986; Vautard et al. 1992). These frequencies are often called the temporal empirical orthogonal functions (T-EOFs) and the way in which the T-EOFs change through time is described by the temporal principal components (T-PCs; Dickinson et al. 2014). When combined linearly, the T-EOFs and the T-PCs form reconstructed components (RCs) which refashion oscillatory modes, noise, and phase information in hydrologic time series. Typically, the first 10 RCs (1–10) are assessed with hydrologic time series because they often account for nearly 100% of the variability in the original time series (Hanson et al. 2004). To determine which RCs are statistically significant against a red-noise null hypothesis, a Ghil and Mo significance test is applied (Ghil and Mo 1991) using HydroClimATe. For the groundwater time series, composite RCs were created by taking only the statistically significant RCs and grouping and summing them together according to the climate variability period ranges of interest: 15–30 years (PDO-like), 6–10 years (NAO-like), 2–7 years (ENSO-like), 2–6 years (EA/SCAND-like) and < 1–4 years (PNA-like).

The CWT is useful to analyze nonstationary signals with variability in both amplitude and frequency, as it exposes dominant modes of variability with time evolving frequencies, which is commonly applied in hydrology (Torrence and Compo 1998; Holman et al. 2011; Kuss and Gurdak 2014; Neves et al. 2016). As defined by Daubechies (1990), CWT is the convolution of the signal with a scaled and translated version of the wavelet function. This method is implemented in MATLAB using the Morlet wavelet described in Torrence and Compo (1998). The Morlet wavelet is advantageous due

Table 2 Descriptive attributes for the location of groundwater observation points in the California Coastal Basins aquifer system. The 'site ID' identifies the aquifer name (CA), the site type (GW for groundwater), and the location (01–08 from northwest to southeast)

Site ID	Location	Site number	Latitude	Longitude
CA GW 01	Humboldt	405702N1241874W001	40.5702	−124.1874
CA GW 02	Napa	385926N1225938W001	38.5926	−122.5938
CA GW 03	Half Moon Bay	374643N1224317W001	37.4643	−122.4317
CA GW 04	San Martin	370881N1216003W001	37.08806	−121.60031
CA GW 05	Santa Barbara	342,630,119,442,301	34.4419	−119.7402
CA GW 06	Ventura	344,156,119,184,801	34.6985	−119.3136
CA GW 07	Los Angeles	340,535,117,573,501	34.0930	−117.9597
CA GW 08	San Bernardino	340,655,117,184,006	34.1151	−117.3116

Table 3 Descriptive attributes for the location of groundwater observation points in Portugal's coastal aquifer system. The 'site ID' identifies the aquifer name (PT), the site type (GW for groundwater), and the location (01–08 from northwest to southeast)

Site ID	Location	Site number	Latitude	Longitude
PT GW 01	Cretacico de Aveiro (O2)	162A/9	−8.7118256	40.753993
PT GW 02	Cretacico de Aveiro (O2)	174/2	−8.6676507	40.742662
PT GW 03	Leirosa – Monte Real (O10)	249/4	−8.8843293	40.055807
PT GW 04	Leirosa – Monte Real (O10)	261/117	−8.854263	40.094272
PT GW 05	Quarteira (M7)	605/303	−8.1342549	37.12038
PT GW 06	Campina de Faro (M12)	606/647	−8.0515888	37.064728
PT GW 07	Campina de Faro (M12)	611/230	−7.9481014	37.048967
PT GW 08	São João da Venda-Quelfes (M10)	607/484	−7.7941745	37.06265

to the equivalence between scale and the equivalent Fourier period (Sang 2013). Once computed, the CWT spectrum illustrates the temporal distribution of the power (variance) as a function of the period (scale), over the 30 years of analysis. The 5% significance levels, indicated by white contours, are computed using a Chi-square test against a red noise spectrum as the null hypothesis and the cone of influence indicated by black lines delimits the regions where results are less reliable. The CWT support and add a temporal component to the dominant frequencies identified by the SSA.

The wavelet coherence is a powerful method used to identify common time-localized oscillatory behaviors between climate indices and groundwater level time series. The algorithm described by Grinsted et al. (2004) is used to compute a 95% confidence level of the WTC. Phase relationships are shown by arrows in the regions of high coherence and their orientation indicate the relative lag between components. Horizontal arrows pointing to the right show in-phase relationships (positive correlation), while arrows pointing to the left are out of phase (negative correlation; Fu et al. 2012). Causality between the two time series can be implied in regions with large common power and consistent phase relationships (Torrence and Webster 1998).

Results

Percent variance of climate variability signals in groundwater levels

Results of the SSA show that all groundwater level time series contain statistically significant oscillations, which are potentially related to the PDO, ENSO, and PNA in California and NAO, EA and SCAND in Portugal—Fig. 5; Tables S1–S2 of the electronic supplementary material (ESM). Plots of the individual significant oscillations corresponding to the periods identified in Fig. 5 are here omitted for the sake of simplicity, but examples can be found in the HydroClimATe software user guide (Dickinson et al. 2014) and Neves et al. (2016). In California, the largest amounts of groundwater level variance (36–77%) have signals consistent with PDO periodicities (15–30-year cycles). The PDO 30-year frequency is equal to the record length analyzed; therefore, statistically significant 30-year signals may not be fully identified due to the limited length of the data records. Modes of variability consistent with PNA periodicities (<1–4-year cycles), which incorporate both a seasonal (0.5-year) and annual (1-year) signal, account for 11–66% of groundwater level variability. ENSO-like 2–7-

Table 4 Descriptive attributes for the groundwater record and hydrology in the California Coastal Basins aquifers system. The hydrologic soil group categories are: *A* for sandy and gravelly textures, *B* for loamy sand or sandy loam textures, *C* for loamy and silty textures, and *D* for clayey textures. *N/A* = information not available. Sampling rate: *Q* for quarterly, *M* for monthly

Site ID	Starting Year	Ending Year	Length of record (years)	Sampling rate	Hydrologic soil group	Well use	Mean piezometric level (m)
CA GW 01	1989	2019	30	Q	B	Residential	6.32
CA GW 02	1989	2019	30	Q	B	Residential	113.40
CA GW 03	1989	2019	30	Q	B	Irrigation	14.39
CA GW 04	1989	2019	30	M	B	Observation	75.21
CA GW 05	1989	2019	30	M	B	Observation	35.72
CA GW 06	1982	2012	30	Q	B	Observation	1125.33
CA GW 07	1984	2014	30	M	N/A	Observation	69.83
CA GW 08	1989	2019	30	M	A	Observation	286.29
Aquifer average:							215.81

Table 5 Descriptive attributes for the groundwater record and hydrology of groundwater wells in Portugal's coastal aquifer system. The hydrologic soil group categories are: Cambissolos cromicos calcarios (*BCA*), Cambissolos humicos rochas sedimentares (*Bh*), Fluvissolos eutricos (*Je*), Podzois orticos (*Po*), and Solonchaks gleizados (*Zg*). Sampling rate: *M* monthly

Site ID	Starting year	Ending year	Length of record (years)	Sampling rate	Hydrologic soil group	Well use	Mean piezometric level (m)
PT GW 01	1989	2019	30	M	Zg, Bh, Je	Observation	−0.10
PT GW 02	1989	2019	30	M	Zg, Bh, Je	Observation	−10.86
PT GW 03	1989	2019	30	M	Po	Observation	23.03
PT GW 04	1989	2019	30	M	Po	Observation	50.40
PT GW 05	1989	2019	30	M	BCA	Observation	12.12
PT GW 06	1989	2019	30	M	BCA, Po	Observation	−2.85
PT GW 07	1989	2019	30	M	BCA, Po	Observation	3.23
PT GW 08	1989	2019	30	M	BCA	Observation	6.56
Aquifer average:							10.19

year cycles, are represented in 4–63% of groundwater variability. In Portugal, the largest amounts of variance in groundwater level (17–63%) have signals consistent with NAO periodicities (6–10-year cycles), yet this is spatially variable across the country (Table S2 of the ESM). The NAO signal is most evident in southern Portugal, accounting for 45–54% (50.75% on average) of groundwater variability. The EA/SCAND-like 2–6-year cycles, account for 8–54% of variability and their joint impact on variance is 33.25% on average in the north and 13.25% on average in the south.

Low-frequency patterns (PDO and NAO) account, on average, for 52.75 and 46.25% of groundwater variability, respectively. EA/SCAND and ENSO, which have the most comparable average periodicity between the two countries, drive substantial variability in California (4–63%) and Portugal (8–54%). These high-frequency signals may be coupled with the low-frequency patterns. Results of the SSA presented similar periods (years) between ENSO-like and PNA-like signals and overlapping NAO-like and EA/SCAND-like signals, indicating interactions between the two systems. Spatially, groundwater RCs with the highest variability were predominantly in northern Portugal, whereas RCs with >50% variability were predominantly located in southern and central California. Results of the SSA show that climate variability signals are captured in the response of groundwater level in both California and Portugal.

Continuous wavelet transform of groundwater levels

The normalized wavelet power spectra of groundwater levels (Fig. 6) across aquifers support results from the SSA and illustrate anomalous events, such as extreme wet (red) and dry (white or blue, or lack of a signal) periods. Anomalously wet precipitation events in 1998 and 2007 are evidenced by the power concentration in the annual (1 year) and 4–8-year bands in California (Fig. 6a,b). Groundwater records also display a division of pre and post 2005 hydroclimatic events. In Portugal, records display prolonged statistically significant oscillations in 2–4 and 4–8-year bands (Fig. 6c,d). The strongest small-scale patches of known anomalously wet years occur in 1996, 2000 and 2010.

Coherence between climate indices and groundwater level

The wavelet coherence between climate indices and groundwater levels are shown in Fig. 7. In order to relate extreme hydroclimatic events and climate variability indices, yellow vertical lines marking major droughts in California (1987–1992, 2001–2002, 2007–2009, and 2012–2016; USGS Water Science Center 2020) and Portugal (1992, 1995, 2004–2005, and 2017; IPMA 2020) are superimposed onto the WTC plots. These lines of episodic drought segment the WTC plots into windows with discrete coherence patterns. Coupling between different climate patterns are identified by the synchronization of coherence patches across patterns at specific periods.

Despite localized hydrogeological differences, every piezometer in California expresses coherence with the ENSO signal, although significant patches of both PDO and PNA are present (Fig. 7a–f). ENSO's strongest patches occur in the 2–4-year band, consistent with the SSA periodicities. All groundwater records in California capture an extreme precipitation event linked to El Niño during the 1997–1998 water year which resulted in record rainfall, which is most obvious in the 0.25–1-year band.

In Portugal, the NAO has a strong coherence with groundwater levels across the entire country (Fig. 7g–l). The EA's 2–4-year periodicity and the SCAND 4–8-year period have the most significant coherence throughout. Coherence patches of

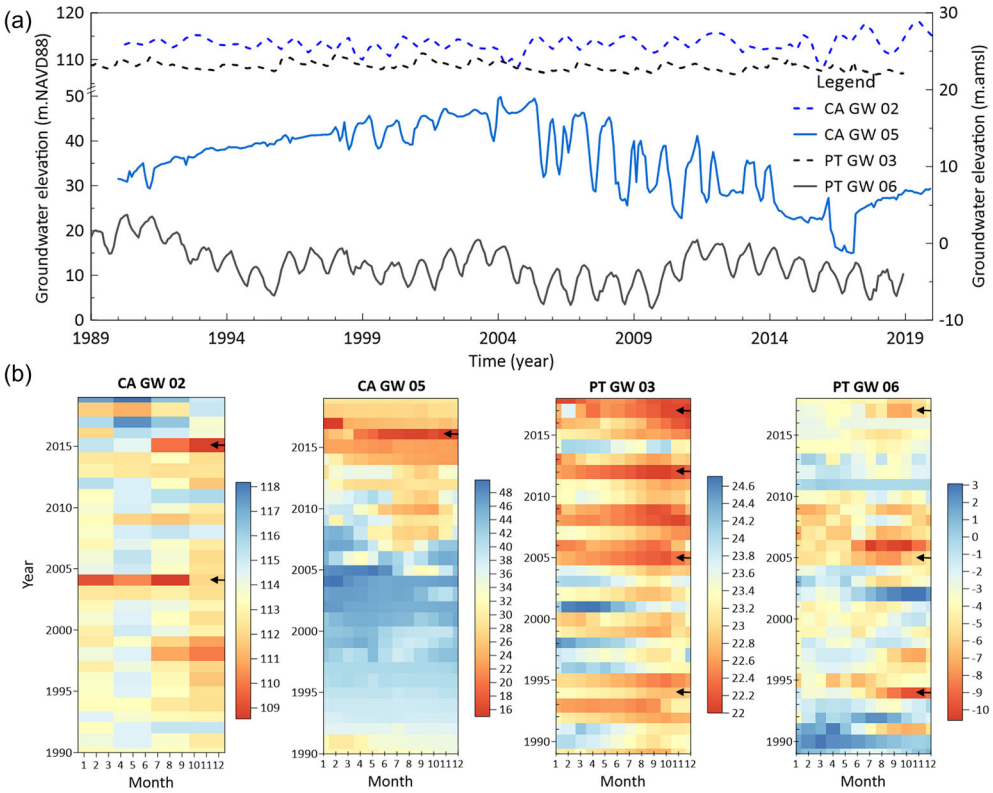

Fig. 4 **a** Groundwater level time series of selected observation points, one located in a northern and southern aquifer system in each country: CA GW 02 in Napa and CA GW 05 in Santa Barbara in California, PT GW 03 in Leirosa (249/4) and PT GW 06 in Campina de Faro (606/647) in Portugal. **b** 30-year time series of groundwater level evolution. Arrows indicate major droughts (IPMA 2020; USGS Water Science Center 2020)

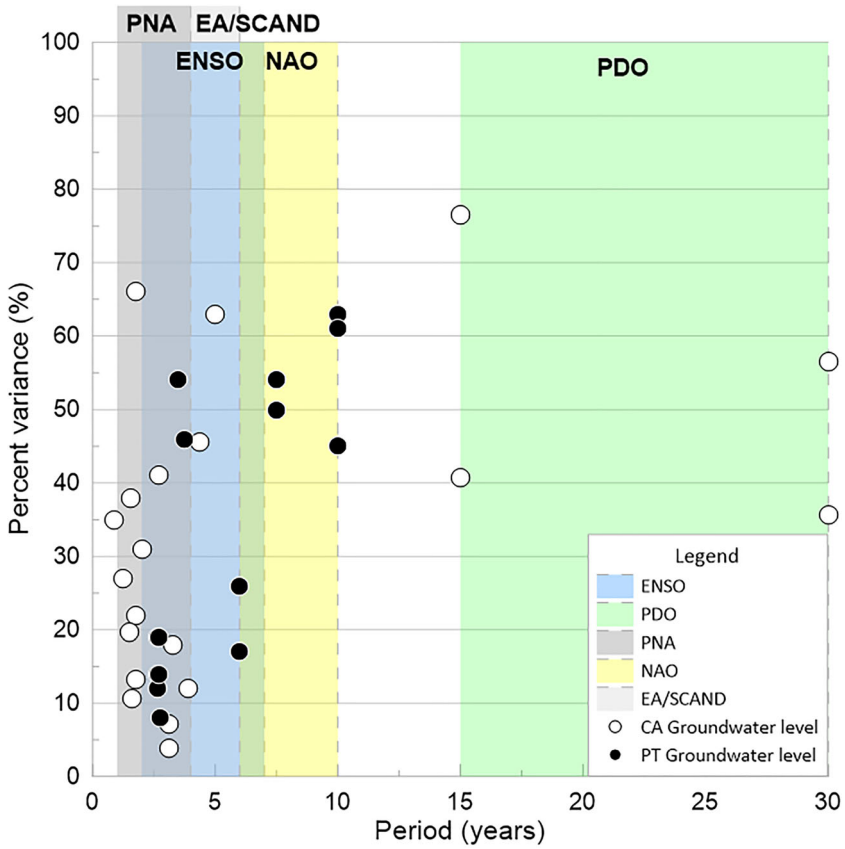

Fig. 5 Percent variance (%) and period (years) of composite groundwater reconstructed components (RCs) in California Coastal Basins aquifers and Portugal's coastal aquifer system

NAO with longer periods, exceeding 4 years are always in an anti-phase, thus NAO– is negatively correlated with groundwater level. As previously described, NAO– results in above-average precipitation in southern Europe. Groundwater records exhibit a significant NAO patch with an anti-phase relationship before 2002, at periods of 1 and 4–8 years, consistent with a NAO event occurring. Significant synchronized patches appear to be linked to EA and SCAND around 2000 (in the 2–4-year time band) in northern Portugal, indicating interactions between these three modes. The dominant SCAND pattern at PT GW 03 is consistent with the SSA RCs' variability with the EA/SCAND frequency which persists from 1996 to 2012. In the Algarve, coherence with the NAO appears in distinct patches in the 4–8-year band 1996–2002, and in the 1-year band around 2014. Significant coherence with the EA is most evident after 2006, at periods of 2–4 years and the SCAND's strongest frequency is between 4 and 8 years. Overall, in Portugal the Scandinavian pattern occupies the largest significant patches of coherence, which often persist for over a decade in the groundwater record. While SCAND does have the broadest influence in Portugal, it is difficult to distinguish the SCAND frequency from that of the EA and NAO.

Discussion

Hydroclimatic teleconnections

Hydroclimatic teleconnections account for a significant amount of groundwater level variability in both California and Portugal. On average, the largest amount of groundwater level variability is attributed to lower frequency patterns, PDO (52.75%) in California and NAO (46.25%) in Portugal. These results are consistent with findings from Gurdak et al. (2007), Kuss (2011) and Velasco et al. (2017), where longer-term climate variations in California aquifers account for greater amounts of variance in hydrologic time series than high frequency (shorter-term) climate variations. In Portugal, the dominance of NAO variability is also reinforced by Neves et al. (2019b) who found that NAO is the primary driver of hydrological variability in the country. Other authors studying the relationship between the NAO, groundwater variability and river flow had similar findings to the SSA results presented earlier, that NAO has stronger influence in the south of Portugal (Gámiz-Fortis et al. 2002). While the impact of climate variability signals is evidenced, aquifers in the Algarve are exploited for agriculture, this groundwater level variability, which is not explained by teleconnections, can be due to the anthropogenic influence, through abstraction and indirect recharge (from irrigation).

A concentration of ENSO-like signals in southern California is supported by previous studies that show a strong influence of ENSO on winter precipitation anomalies of the southern US (Kiladis and Diaz 1989; Kurtzman and Scanlon 2007; Ropelewski and Halpert 1986). However, less detection of the higher frequency ENSO signal in the groundwater levels than that of the PDO signal, may also be attributed to the relative greater damping of the higher frequencies in the relatively thick vadose zones of the study area (Corona et al. 2018).

In Portugal, the joint impact of higher frequency signals (EA and SCAND) on variance is 33.25% on average in the north and 13.25% on average in the south, similar to findings from Neves et al. (2019b). However due to their overlapping periodicities, EA and SCAND are difficult to distinguish. Overlapping periodicities of two climate variability modes in both study areas (ENSO and PNA in California and EA and SCAND in Portugal) highlights an important limitation of using SSA to identify influence from specific modes of climate variability on groundwater level. Anomalous events such as the heavy precipitation years of 1998 and 2007, coincide with known ENSO events in California, and the occurrence and impact of drought appear in groundwater level records in Portugal from 2004 to 2005.

Coherence between climate indices and groundwater levels and drought

Previous studies suggest that a positive PDO phase can intensify El Niño, driving a more robust pattern of wetter winters in the southern US (Brown and Comrie 2004; Gershunov and Barnett 1998). The reverse occurs for the negative phase. In this study the coherence plots show that in northern and central California, a strong PDO+ coherence with a 4–8 period precedes drought events. Small yet significant patches of PDO– coherence occur between drought bars in southern California around a 1-year period in 2000 and 2005, which align with the PDO– ENSO– coupling events (Fig. 3). The implications of El Niño (ENSO+) on drought occurrence are also evident across the state of California. In northern California, El Niño coherence with a 4–8-year period persists throughout major drought events. The synchronization of PDO+ and El Niño also becomes most evident in northern California, marking interactions between both patterns and drought events. The PNA loosely follows the phasing of ENSO and often occurs before or even during periods of drought.

In Portugal, patches of NAO– coherence are most significant in the 4–8-year band. Yet a 1-year-period band is in-phase (NAO+) around 2000, where Fig. 3 confirms that NAO was in a positive phase in 2000. This variability could be attributed to the influenceability of shorter period signals or the hydrogeographic composition of the aquifer. A significant NAO event occurs before the 2004–2005 drought episode and coupling between NAO+ and EA– are centered in the middle of the drought episode (Fig. 3). EA and SCAND coherence patterns are tapered near droughts events. This behavior is most obvious in the 4–8-year period in southern Portugal,

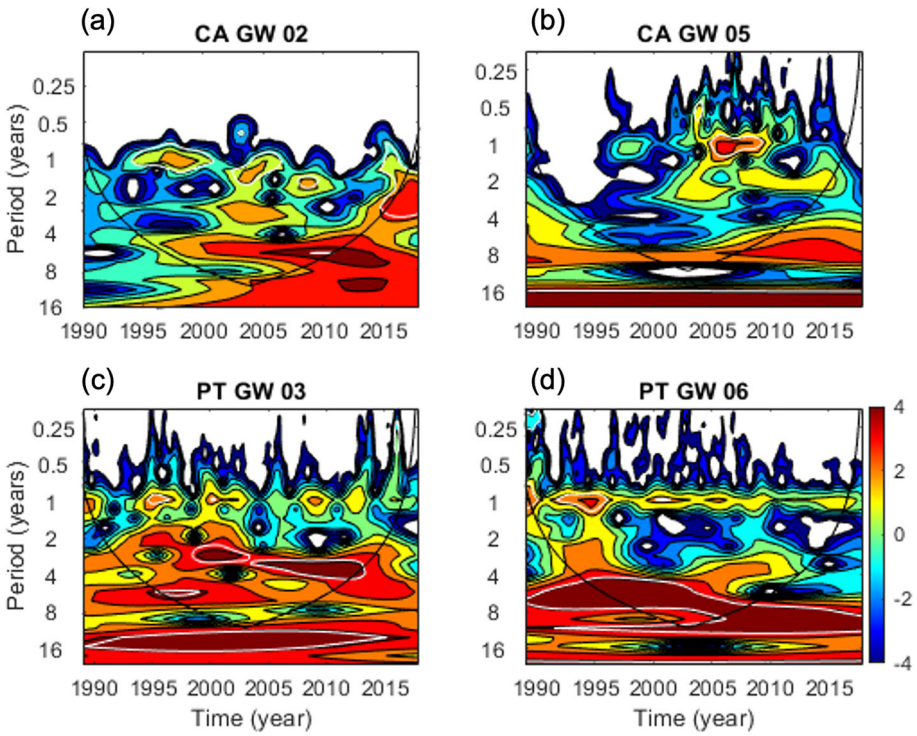

Fig. 6 **a**–**d** Wavelet power spectra of select groundwater observation points computed using a Morlet wavelet and normalized by $1/\sigma^2$, where σ^2 is the variance of the time series. The white contours enclose regions that are of greater than 95% confidence levels. The black lines delimit the cone of influence, where zero padding has reduced the variance

although it occurs in all records. The impact of climate variability coupling is evidenced throughout both aquifers' systems in California and Portugal although drought incidence and behavior seem to be different in California, where sustained droughts can last up to 6 years.

Comparison between California and Portugal

Findings from this research present both distinct similarities and differences between the two systems. Coastal aquifers in both California and Portugal are unequivocally impacted by modes of climate variability. Lower frequency patterns (NAO with 8-years and PDO with 22-years on average) were the dominant driver of variability in groundwater level. Two patterns had comparable periodicities (EA/SCAND with a 3-year period and ENSO with a 3.4-year period) and drove up to 54 and 63% of groundwater variability, respectively. Longer-term patterns also influence the shorter-term (high frequency) patterns during coupling events. In the SSA, overlapping frequencies occurred for both patterns in California and Portugal, potentially masking one signal and strongly expressing another. Coupling events were also evidenced in the WCT, aligning with some mode interactions (presented in Fig. 3). In both regions, specific coupling arrangements (phase combinations) are associated with extreme events such as anomalously wet conditions (PDO+ ENSO+) or drought (NAO+ EA–). In response to the initial research question posed at the beginning of this study, a common response to climate pattern couplings in Mediterranean climates is indeed found.

However, some noticeable differences between California and Portugal are also presented throughout this work. Firstly, the highest percent of groundwater level variability was opposing in California and Portugal. In the SSA, RCs with the highest variability were predominantly in northern Portugal, while California groundwater RCs with >50% variability were predominantly in southern and central California. This could be attributed to a mix of the precipitation regime, the sensitivity to hydrogeological properties and the local-scale dynamics of the individual and coupled climate patterns.

Implications for water management

Water resources are increasingly threatened in the Anthropocene (Van Loon et al. 2016), as rising drying trends catalyze droughts (Dai 2013) and deplete groundwater reserves (Famiglietti 2014; Ferguson and Gleeson 2012), posing further urgency around global water security. Groundwater is predominantly a renewable freshwater resource, when managed properly. It can ensure a long-term supply for human use and ecosystem function even amidst increasing demands and anticipated effects of global climate change. However, aquifers are strongly influenced by climate variability, and recharge rates may widely vary across aquifer systems. Hence, understanding the response of aquifer systems to climate patterns is extremely important in the context of climate change. Groundwater plays a critical role during droughts because it is very often the main source of potable water for drinking and

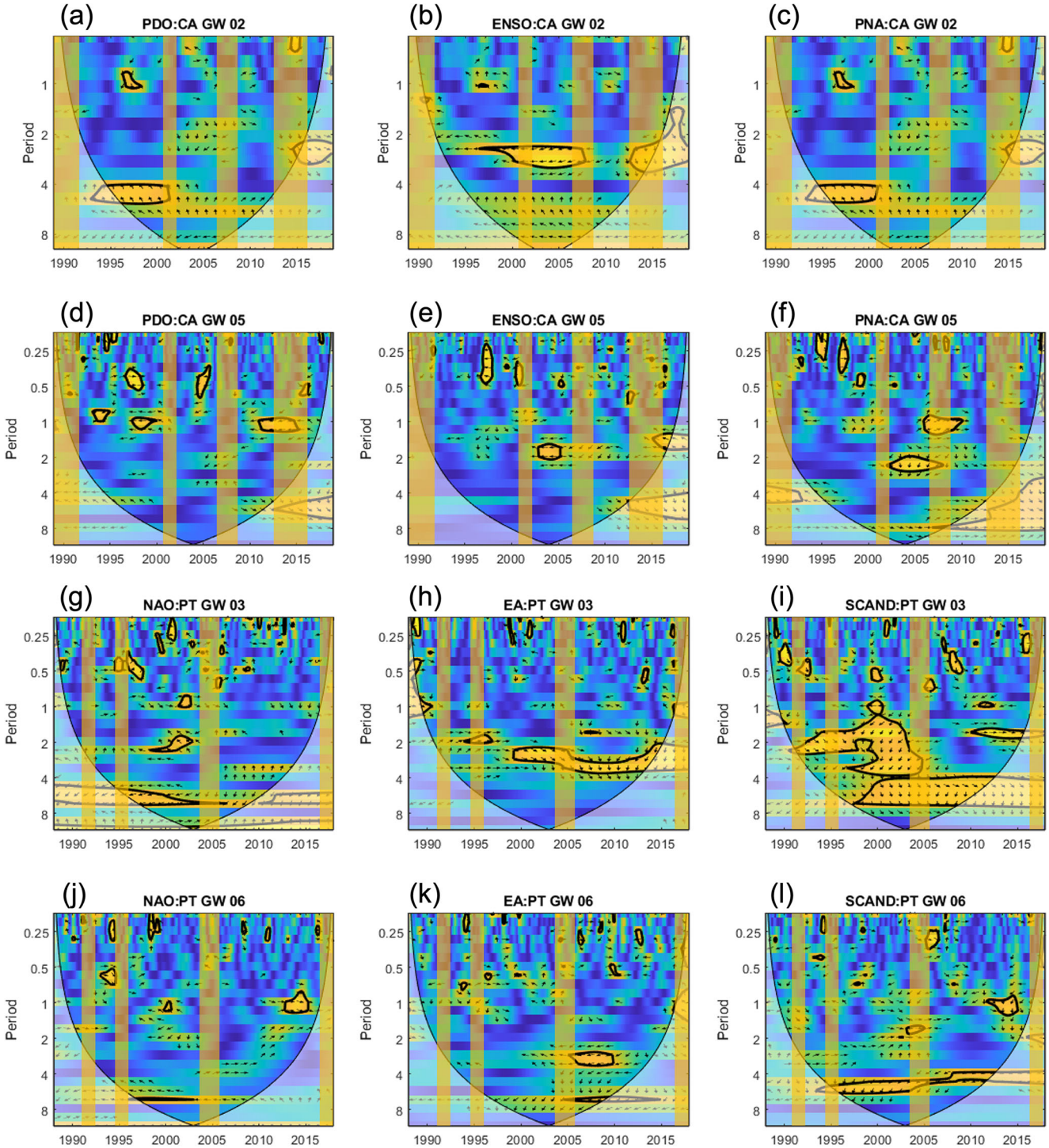

Fig. 7 **a**–**l** Wavelet coherence of time series of select groundwater observation points. The thick black lines are the 5% significance level, while faded "or less intense" colors indicate the cone of influence. Horizontal right-pointing (left-pointing) arrows indicate the in-phase (anti-phase) relationships

irrigation. The evidence on the association of coupled climate patterns and hydrologic extremes found in this study at both Portugal and California may motivate future investigations focusing on the impacts of coupled teleconnections. An integrated forecast system of groundwater availability can benefit from the identification of such couplings, as already recognized in recent studies in Australia (Cleverly et al. 2016; Fan et al. 2020). While the skillful prediction of climate patterns is admittedly difficult due to predominantly stochastic nature of the

atmospheric circulation oscillations, recent progress in coupled oceanic-atmospheric climate models and ensemble production techniques have shown that mid-latitude climate variability does exhibit significant predictability at seasonal scales (Scaife et al. 2014; Athanasiadis et al. 2020). These recent advances in the seasonal and long-term predictability of climate patterns can help to improve drought resilience and have huge potential benefits for water management in Mediterranean and semiarid regions.

Conclusion

The application of SSA to identify and evaluate quasiperiodic signals in groundwater level time series indicates that PDO, ENSO, PNA, NAO, EA, and SCAND have significant influence on groundwater fluctuations across coastal aquifer systems in California (USA) and Portugal. Lower frequency oscillations have a greater influence on hydrologic patterns, with PDO and NAO accounting for the largest amount of variability. While the imprint of high-frequency signals is also evident, the lower frequency signals tend to be better preserved in groundwater level fluctuations.

Interrelationships between climate patterns, groundwater level variability and drought occurrence are evidenced through the application of wavelet transform methods. Coupled climate modes coincide with hydrological droughts throughout the 30-year time span of this study, where specific mode combinations (NAO+ EA– and drought; NAO– EA+ SCAND+ and heavy precipitation; PDO+ ENSO+ increased precipitation in southern CA; PDO– ENSO– increased precipitation in northern CA) drive groundwater level anomalies. The strongest covariability between climate patterns and groundwater levels occurs in the following dominant periods—4–8 years for PDO, 2–4 years for ENSO, 1–2 years for PNA, 5–8 years band for NAO, 2–4 years for EA and 2–8 years for SCAND. Frequencies from EA and SCAND are often coupled with NAO signals.

This work is the first to provide a comparative statistical and analytical analysis of climate mode coupling effects on coastal aquifers of California and Portugal, offering insights for coastal aquifers in vulnerable regions around the world, including Mediterranean climates and semiarid regions. It also advances the current understanding of hydro-climatological behavior of aquifers under increasing climate uncertainty. Precipitation and groundwater level teleconnections with large-scale ocean–atmosphere oscillation systems provide useful information for water management. Predicting the onset of groundwater drought is of paramount importance, as groundwater resources are often used as buffers against water shortages and droughts are expected to become increasingly frequent and severe in semiarid regions. Couplings of climate patterns and their association with extreme events identified in both Portugal and California offer a potential source of long-term forecasting that needs to be further explored. A deepened understanding of how climate variability patterns and the coupling between modes influence groundwater storage will assist future projects of groundwater availability and sustainability.

Supplementary Information The online version contains supplementary material available at https://doi.org/10.1007/s10040-022-02470-z.

Acknowledgements We are grateful for the constructive comments and suggestions of three anonymous reviewers and the associate editor, which helped to improve the manuscript.

Funding This publication is partially supported by FCT-project UIDB/50019/2020 – IDL (Instituto Dom Luiz).

Declarations

Conflict of interest There are no conflicts of interest.

References

Almeida CC, Mendonça JL, Jesus MR, Gomes AJ (2000) Sistemas aquíferos de Portugal continental [Aquifer systems of continental Portugal]. Report, INAG, Instituto da Água Lisboa, Lisbon

APA (2020) Sistemas aquíferos. Sistema Nacional de Informação de Recursos Hídricos [National Information system for water resources]. https://snirh.apambiente.pt/. Accessed 12 Dec 2019

Asoka A, Gleeson T, Wada Y, Mishra V (2017) Relative contribution of monsoon precipitation and pumping to changes in groundwater storage in India. Nat Geosci 10:109–117. https://doi.org/10.1038/ngeo2869

Athanasiadis PJ, Yeager S, Kwon Y-O, Bellucci A, Smith DW, Tibaldi S (2020) Decadal predictability of North Atlantic blocking and the NAO. NPJ Clim Atmos Sci 3:20. https://doi.org/10.1038/s41612-020-0120-6

Barco J, Hogue TS, Girotto M, Kendall DR, Putti M (2010) Climate signal propagation in southern California aquifers. Water Resour Res 46:1–19. https://doi.org/10.1029/2009WR008376

Barnston AG, Livezey RE (1987) Classification, seasonality and persistence of low-frequency atmospheric circulation patterns. Mon Weather Rev 115:1083–1126. https://doi.org/10.1175/1520-0493(1987)115<1083:CSAPOL>2.0.CO;2

Beebee RA, Manga M (2004) Variation in the relationship between snowmelt runoff in Oregon and ENSO and PDO. J Am Water Resour Assoc 40:1011–1024. https://doi.org/10.1111/j.1752-1688.2004.tb01063.x

Bove MC, O'Brien JJ, Eisner JB, Landsea CW, Niu X (1998) Effect of El Niño on US landfalling hurricanes, revisited. Bull Am Meteorol Soc 79:2477–2482. https://doi.org/10.1175/1520-0477(1998)079<2477:EOENOO>2.0.CO;2

Brabets TP, Walvoord MA (2009) Trends in streamflow in the Yukon River basin from 1944 to 2005 and the influence of the Pacific decadal oscillation. J Hydrol 371:108–119. https://doi.org/10.1016/j.jhydrol.2009.03.018

Broomhead DS, King GP (1986) Extracting qualitative dynamics from experimental data. Phys D Nonlinear Phenom 20:217–236. https://doi.org/10.1016/0167-2789(86)90031-X

Brown DP, Comrie AC (2004) A winter precipitation "dipole" in the western United States associated with multidecadal ENSO variability. Geophys Res Lett 31:1–4. https://doi.org/10.1029/2003GL018726

Bueha C, Nakamurab H (2007) Scandinavian pattern and its climatic impact. Q J R Meteorol Soc 133:2117–2131. https://doi.org/10.1002/qj.173

CA DWR (2018) California Statewide Groundwater Elevation Monitoring (CASGEM). https://www.casgem.water.ca.gov/. Accessed 12 Dec 2019

Cleverly J, Eamus D, Luo Q, Restrepo Coupe N, Kljun N, Ma X, Ewenz C, Li L, Yu Q, Huete A (2016) The importance of interacting climate modes on Australia's contribution to global carbon cycle extremes. Sci Rep 6:23113. https://doi.org/10.1038/srep23113

Corona CR, Gurdak JJ, Dickinson JE, Ferré TPA, Maurer EP (2018) Climate variability and vadose zone controls on damping of transient recharge. J Hydrol 561:1094–1104. https://doi.org/10.1016/j.jhydrol.2017.08.028

Cui T, Raiber M, Pagendam D, Gilfedder M, Rassam D (2017) Response of groundwater level and surface-water/groundwater interaction to climate variability: Clarence-Moreton Basin, Australia. Hydrogeol J 26:593–614. https://doi.org/10.1007/s10040-017-1653-6

Cui Y, Liao Z, Wei Y, Xu X, Song Y, Liu H (2020) The response of groundwater level to climate change and human activities in Baotou City, China. Water 12:1078. https://doi.org/10.3390/w12041078

Dai A (2013) Increasing drought under global warming in observations and models. Nat Clim Chang 3:52–58. https://doi.org/10.1038/nclimate1633

Daubechies I (1990) The wavelet transform, time-frequency localization and signal analysis. IEEE Trans Inf Theory 36:961–1005. https://doi.org/10.1109/18.57199

De Vita P, Allocca V, Manna F, Fabbrocino S (2012) Coupled decadal variability of the North Atlantic oscillation, regional rainfall and karst spring discharges in the Campania region (southern Italy). Hydrol Earth Syst Sci 16:1389–1399. https://doi.org/10.5194/hess-16-1389-2012

del V Venencio M, García NO (2011) Interannual variability and predictability of water table levels at Santa Fe Province (Argentina) within the climatic change context. J Hydrol 409:62–70. https://doi.org/10.1016/j.jhydrol.2011.07.039

Derbyshire SH, Beau I, Bechtold P, Grandpeix J-Y, Piriou J-M, Redelsperger J-L, Soares PMM (2004) Sensitivity of moist convection to environmental humidity. Q J R Meteorol Soc 130:3055–3079. https://doi.org/10.1256/qj.03.130

Dickinson JE, Hanson RT, Predmore SK (2014) HydroClimATe: hydrologic and climatic analysis toolkit. Tech Methods. https://doi.org/10.3133/tm4a9

Enfield DB, Mestas-Nufiez AM, Trinble PJ (2001) The Atlantic multidecadal oscillation and its relation to rainfall and river flows in the continental U.S. Geophys Res Lett 28:2077–2080

Famiglietti JS (2014) The global groundwater crisis. Nat Clim Chang 4:945–948. https://doi.org/10.1038/nclimate2425

Fan L, Guan H, Cai W, Rofe CP, Xu J (2020) A 7-year lag precipitation teleconnection in South Australia and its possible mechanism. Front Earth Sci 8:1–12. https://doi.org/10.3389/feart.2020.553506

Ferguson G, Gleeson T (2012) Vulnerability of coastal aquifers to groundwater use and climate change. Nat Clim Chang 2:342–345. https://doi.org/10.1038/nclimate1413

Fu C, James AL, Wachowiak MP (2012) Analyzing the combined influence of solar activity and El Niño on streamflow across southern Canada. Water Resour Res 48. https://doi.org/10.1029/2011WR011507

Gámiz-Fortis SR, Pozo-Vázquez D, Esteban-Parra MJ, Castro-Díez Y (2002) Spectral characteristics and predictability of the NAO assessed through singular spectral analysis. J Geophys Res Atmos 107:ACL 11-1–ACL 11-15. https://doi.org/10.1029/2001JD001436

Gershunov A, Barnett TP (1998) Interdecadal modulation of ENSO teleconnections. Bull Am Meteorol Soc 79:2715–2725

Gershunov A, Barnett TP, Cayan DR (1999) North Pacific interdecadal oscillation seen as factor in ENSO-related North American climate anomalies. EOS Trans Am Geophys Union 80:25. https://doi.org/10.1029/99EO00019

Ghil M (2002) Natural climate variability. In: Encyclopedia of global environmental change. Wiley, Chichester, UK, pp 544–549

Ghil, Mo (1991) Intraseasonal oscillations in the global atmosphere, part I: Northern Hemisphere and tropics. J Atmos Sci 48(5):752. https://doi.org/10.1175/1520-0469(1991)048<0752:ioitga>2.0.co;2

Giannini A, Saravanan R, Chang P (2003) Oceanic forcing of Sahel rainfall on interannual to interdecadal time scales. Science 302(5647):1027–1030. https://doi.org/10.1126/science.1089357

Giorgi F (2006) Climate change hot-spots. Geophys Res Lett 33:1–4. https://doi.org/10.1029/2006GL025734

Gleeson T, Wada Y, Bierkens MFP, Van Beek LPH (2012) Water balance of global aquifers revealed by groundwater footprint. Nature 488:197–200. https://doi.org/10.1038/nature11295

Grinsted A, Moore JC, Jevrejeva S (2004) Application of the cross wavelet transform and wavelet coherence to geophysical time series. Nonlinear Process Geophys 11:561–566. https://doi.org/10.5194/npg-11-561-2004

Gurdak JJ (2017) Groundwater: climate-induced pumping. Nat Geosci 10:71–72. https://doi.org/10.1038/ngeo2885

Gurdak JJ, Hanson RT, McMahon PB, Bruce BW, McCray JE, Thyne GD, Reedy RC (2007) Climate variability controls on unsaturated water and chemical movement, High Plains aquifer, USA. Vadose Zone J 6:533–547. https://doi.org/10.2136/vzj2006.0087

Hanson RT, Newhouse MW, Dettinger MD (2004) A methodology to asess relations between climatic variability and variations in hydrologic time series in the southwestern United States. J Hydrol 287:252–269. https://doi.org/10.1016/j.jhydrol.2003.10.006

Hanson RT, Dettinger MD, Newhouse MW (2006) Relations between climatic variability and hydrologic time series from four alluvial basins across the southwestern United States. Hydrogeol J 14:1122–1146. https://doi.org/10.1007/s10040-006-0067-7

Holman IP, Rivas-Casado M, Bloomfield JP, Gurdak JJ (2011) Identifying non-stationary groundwater level response to North Atlantic Ocean-atmosphere teleconnection patterns using wavelet coherence. Hydrogeol J 19:1269–1278. https://doi.org/10.1007/s10040-011-0755-9

Hurrell JW (1995) Decadal trends in the North Atlantic oscillation: regional temperatures and precipitation. Science 269:676–679

IPCC (2001) In: Houghton JT, Ding Y, Griggs DJ, Noguer M, Linden PJ, van der Dai X, Maskell K, Johnson CA (eds) Contribution of Working Group I to the third assessment report of the Intergovernmental Panel on Climate C. Cambridge Univ Press, New York, 94 pp

IPMA (2020) Instituto Português do Mar a e da Atmosfera [Portuguese Institute of the Sea and Atmosphere]. https://www.ipma.pt/

Jolly WM, Cochrane MA, Freeborn PH, Holden ZA, Brown TJ, Williamson GJ, Bowman DMJS (2015) Climate-induced variations in global wildfire danger from 1979 to 2013. Nat Commun 6:1–11. https://doi.org/10.1038/ncomms8537

Joshi N, Kalra A, Lamb KW (2020) Land–ocean–atmosphere influences on groundwater variability in the South Atlantic–Gulf region. Hydrology 7:71. https://doi.org/10.3390/hydrology7040071

Kalimeris A, Ranieri E, Founda D, Norrant C (2017) Variability modes of precipitation along a Central Mediterranean area and their relations with ENSO, NAO, and other climatic patterns. Atmos Res 198:56–80. https://doi.org/10.1016/j.atmosres.2017.07.031

Kiladis GN, Diaz HF (1989) Global climatic anomalies associated with extremes in the southern oscillation. J Clim 2:1069–1090. https://doi.org/10.1175/1520-0442(1989)002<1069:gcaawe>2.0.co;2

Kottek M, Grieser J, Beck C, Rudolf B, Rubel F (2006) World map of the Köppen-Geiger climate classification updated. Meteorol Zeitschrift 15:259–263. https://doi.org/10.1127/0941-2948/2006/0130

Kundzewicz ZW, Döll P (2009) Will groundwater ease freshwater stress under climate change? Hydrol Sci J 54:665–675. https://doi.org/10.1623/hysj.54.4.665

Kurtzman D, Scanlon BR (2007) El Niño-southern oscillation and Pacific decadal oscillation impacts on precipitation in the southern and central United States: evaluation of spatial distribution and predictions. Water Resour Res 43:1–12. https://doi.org/10.1029/2007WR005863

Kuss AJM (2011) Effects of climate variability on recharge in regional aquifers of the United States. US Geol Surv Fact Sheet 2009–3074

Kuss AJM, Gurdak JJ (2014) Groundwater level response in US principal aquifers to ENSO, NAO, PDO, and AMO. J Hydrol 519:1939–1952. https://doi.org/10.1016/j.jhydrol.2014.09.069

Liu Y, Stanturf J, Goodrick S (2010) Trends in global wildfire potential in a changing climate. For Ecol Manag 259:685–697. https://doi.org/10.1016/j.foreco.2009.09.002

Manna F, Walton KM, Cherry JA, Parker BL (2019) Five-century record of climate and groundwater recharge variability in southern California. Sci Rep 9:1–8. https://doi.org/10.1038/s41598-019-54560-w

Mantua NJ, Hare SR, Zhang Y, Wallace JM, Francis RC (1997) A Pacific Interdecadal climate oscillation with impacts on salmon production. Bull Am Meteorol Soc 78:1069–1079. https://doi.org/10.1175/1520-0477(1997)078<1069:APICOW>2.0.CO;2

Masih I, Maskey S, Mussá FEF, Trambauer P (2014) A review of droughts on the African continent: a geospatial and long-term perspective. Hydrol Earth Syst Sci 18:3635–3649. https://doi.org/10.5194/hess-18-3635-2014

McCabe GJ, Palecki MA, Betancourt JL (2004) Pacific and Atlantic Ocean influences on multidecadal drought frequency in the United States. Proc Natl Acad Sci USA 101:4136–4141. https://doi.org/10.1073/pndoi:as.0306738101

Miranda P, Coelho FES, Tomé AR, Valente MA (2002) 20th century Portuguese climate and climate scenarios. In: Climate change in Portugal: scenarios, impacts and adaptation measures. SIAM project, pp 23–83

Navarra A, Tubiana L (eds) (2013) Regional assessment of climate change in the Mediterranean, vol 3: case studies. In: Advances in global change research. Springer, Heidelberg, Germany

Neves MC, Costa L, Monteiro JP (2016) Climatic and geologic controls on the piezometry of the Querença-Silves karst aquifer, Algarve (Portugal). Hydrogeol J 24:1015–1028. https://doi.org/10.1007/s10040-015-1359-6

Neves MC, Costa L, Hugman R, Monteiro JP (2019a) The impact of atmospheric teleconnections on the coastal aquifers of ria Formosa (Algarve, Portugal). Hydrogeol J 27:2775–2787. https://doi.org/10.1007/s10040-019-02052-6

Neves MC, Jerez S, Trigo RM (2019b) The response of piezometric levels in Portugal to NAO, EA, and SCAND climate patterns. J Hydrol 568:1105–1117. https://doi.org/10.1016/j.jhydrol.2018.11.054

NOAA (2019) National Oceanic and Atmospheric Administration. Climate Prediction Center. http://www.cpc.ncep.noaa.gov. Accessed March 2022

NOAA (2020a) Climate monitoring: teleconnections. https://www.ncdc.noaa.gov/teleconnections/. Accessed March 2022

NOAA (2020b) Multivariate ENSO index version 2 (MEI.v2). Physical Sciences Laboratory. https://psl.noaa.gov/enso/mei/. Accessed March 2022

Norman SP, Taylor AH (2003) Tropical and North Pacific teleconnections influence fire regimes in pine-dominated forests of north-eastern California, USA. J Biogeogr 30:1081–1092. https://doi.org/10.1046/j.1365-2699.2003.00889.x

Nathan J., Mantua Steven R., Hare Journal of Oceanography 58(1) 35-44 https://doi.org/10.1023/A:1015820616384

Perez-Valdivia C, Sauchyn D, Vanstone J (2012) Groundwater levels and teleconnection patterns in the Canadian prairies. Water Resour Res 48:1–13. https://doi.org/10.1029/2011WR010930

Planert M, Williams JS (1995) Ground water atlas of the United States: segment 1 California, Nevada. US Geol Surv Hydrol Invest Atlas 730-B:30

Poveda G, Rojas W, Quinones ML, Velez ID, Mantilla RI, Ruiz D, Zuluaga JS, Rua GL (2001) Coupling between annual and ENSO timescales in the malaria: climate association in Colombia. Environ Health Perspect 109:489. https://doi.org/10.2307/3454707

Romm J (2011) Desertification: the next dust bowl. Nature 478:450–451. https://doi.org/10.1038/478450a

Ropelewski CF, Halpert MS (1986) North American precipitation and temperature patterns associated with the El Niño/southern oscillation (ENSO). Mon Weather Rev 114:2352–2362

Russo TA, Lall U (2017) Depletion and response of deep groundwater to climate-induced pumping variability. Nat Geosci 10:105–108. https://doi.org/10.1038/ngeo2883

Rust W, Holman I, Bloomfield J, Cuthbert M, Corstanje R (2019) Understanding the potential of climate teleconnections to project future groundwater drought. Hydrol Earth Syst Sci 23:3233–3245. https://doi.org/10.5194/hess-23-3233-2019

Sang YF (2013) A review on the applications of wavelet transform in hydrology time series analysis. Atmos Res 122:8–15. https://doi.org/10.1016/j.atmosres.2012.11.003

Scaife AA, Arribas A, Blockley E, Brookshaw A, Clark RT, Dunstone N, Eade R, Fereday D, Folland CK, Gordon M, Hermanson L, Knight JR, Lea DJ, MacLachlan C, Maidens A, Martin M, Peterson AK, Smith D, Vellinga M, Wallace E, Waters J, Williams A (2014) Skillful long-range prediction of European and North American winters. Geophys Res Lett 41:2514–2519. https://doi.org/10.1002/2014GL059637

Scanlon BR, Keese KE, Flint AL, Flint LE, Gaye CB, Edmunds WM, Simmers I (2006) Global synthesis of groundwater recharge in semiarid and arid regions. Hydrol Process 20:3335–3370. https://doi.org/10.1002/hyp.6335

Schubert SD, Suarez MJ, Pegion PJ, Koster RD, Bacmeister JT (2004) On the cause of the 1930s dust bowl. Science 303:1855–1859. https://doi.org/10.1126/science.1095048

Steirou E, Gerlitz L, Apel H, Merz B (2017) Links between large-scale circulation patterns and streamflow in Central Europe: a review. J Hydrol 549:484–500. https://doi.org/10.1016/j.jhydrol.2017.04.003

Stigter TY, Nunes JP, Pisani B, Fakir Y, Hugman R, Li Y, Tomé S, Ribeiro L, Samper J, Oliveira R, Monteiro JP, Silva A, Tavares PCF, Shapouri M, Cancela da Fonseca L, El Himer H (2014) Comparative assessment of climate change and its impacts on three coastal aquifers in the Mediterranean. Reg Environ Chang 14:41–56. https://doi.org/10.1007/s10113-012-0377-3

Taylor RG, Scanlon B, Döll P, Rodell M, van Beek R, Wada Y, Longuevergne L, Leblanc M, Famiglietti JS, Edmunds M, Konikow L, Green TR, Chen J, Taniguchi M, Bierkens MFP, MacDonald A, Fan Y, Maxwell RM, Yechieli Y et al (2013) Ground water and climate change. Nat Clim Chang 3:322–329. https://doi.org/10.1038/nclimate1744

Torrence C, Compo GP (1998) A practical guide to wavelet analysis. Bull Am Meteorol Soc 79:61–78. https://doi.org/10.1175/1520-0477(1998)079<0061:APGTWA>2.0.CO;2

Torrence C, Webster P (1998) The annual cycle of persistence in the El Nino/southern oscillation. Q J R Meteorol Soc 124:1985–2004. https://doi.org/10.1256/smsqj.55009

Tremblay L, Larocque M, Anctil F, Rivard C (2011) Teleconnections and interannual variability in Canadian groundwater levels. J Hydrol 410:178–188. https://doi.org/10.1016/j.jhydrol.2011.09.013

Trigo RM, Valente MA, Trigo IF, Miranda PMA, Ramos AM, Paredes D, García-Herrera R (2008) The impact of North Atlantic wind and cyclone trends on European precipitation and significant wave height in the Atlantic. Ann N Y Acad Sci 1146:212–234. https://doi.org/10.1196/annals.1446.014

Trigo RM, Añel J, Barriopedro D, García-Herrera R, Gimeno L, Nieto R, Castillo R, Allen MR, Massey N (2013) The record winter drought of 2011–12 in the Iberian Peninsula. Bull Am Meteorol Soc 94(9):S41–S45

T. N., Palmer D. L. T., Anderson (1994) The prospects for seasonal forecasting—A review paper. Quarterly Journal of the Royal Meteorological Society 120(518) 755-793 https://doi.org/10.1002/qj.49712051802

United Nations (2016) UN atlas of the oceans. http://www.oceansatlas.org/. Accessed March 2019

USGS (2015) National Water Information System (NWIS). http://waterdata.usgs.gov/nwis. Accessed Dec 2019

USGS Water Science Center (2020) 2012–2016 California Drought: historical perspective. https://ca.water.usgs.gov/california-drought/california-drought-comparisons.html. Accessed March 2022

Van Loon AF, Gleeson T, Clark J, Van Dijk AIJM, Stahl K, Hannaford J, Di Baldassarre G, Teuling AJ, Tallaksen LM, Uijlenhoet R, Hannah DM, Sheffield J, Svoboda M, Verbeiren B, Wagener T, Rangecroft S, Wanders N, Van Lanen HAJ (2016) Drought in the Anthropocene. Nat Geosci 9:89–91. https://doi.org/10.1038/ngeo2646

Vautard R, Yiou P, Ghil M (1992) Singular-spectrum analysis: a toolkit for short, noisy chaotic signals. Phys D Nonlinear Phenom 58:95–126. https://doi.org/10.1016/0167-2789(92)90103-T

Velasco EM, Gurdak JJ, Dickinson JE, Ferré TPA, Corona CR (2017) Interannual to multidecadal climate forcings on groundwater resources of the U.S. west coast. J Hydrol Reg Stud 11:250–265. https://doi.org/10.1016/j.ejrh.2015.11.018

Vicente-Serrano SM, López-Moreno JI, Gimeno L, Nieto R, Morán-Tejeda E, Lorenzo-Lacruz J, Beguería S, Azorin-Molina C (2011) A multiscalar global evaluation of the impact of ENSO on droughts. J Geophys Res Atmos 116:1–23. https://doi.org/10.1029/2011JD016039

Wallace JM, Gutzler DS (1981) Teleconnections in the geopotential height field during the northern hemisphere winter. Mon Weather Rev 109:784–812. https://doi.org/10.1175/1520-0493(1981)109<0784:TITGHF>2.0.CO;2